Synthesis and atomic-level characterization of Ni nanoparticles in Al_2O_3 matrix

D. Kumar,[a] S. J. Pennycook, and A. Lupini
Solid State Division, Oak Ridge National Laboratory, Oak Ridge, Tennessee 37831

G. Duscher, A. Tiwari, and J. Narayan
Center for Advanced Materials and Smart Structures, Department of Materials Science and Engineering, North Carolina State University, Raleigh, North Carolina 27695

(Received 22 April 2002; accepted 5 October 2002)

Single domain magnetic nickel nanocrystals were embedded in alumina matrix using a pulsed-laser deposition technique. Structural characterization carried out at the atomic level using scanning transmission electron microscopy with atomic number contrast (STEM-Z) in conjunction with electron energy loss spectroscopy have revealed that the Ni particles are well separated and have interfaces with the host matrix that are atomically sharp and free of any oxide layer. An excellent correlation was found between particle sizes determined theoretically from magnetization versus field data and experimentally using STEM-Z which indicates the absence of any magnetically dead layers on the Ni nanoparticles within an experimental error of 0.1 monolayer. © *2002 American Institute of Physics.* [DOI: 10.1063/1.1525052]

Nanophase magnetic materials have attracted intense research interest in recent years, driven by their technological importance in magnetic recording, ferrofluid technology, magnetocaloric refrigeration, biomedicine, and biotechnology.[1–9] The nanophase materials in these devices perform more efficiently than their bulk counterparts due to the outstanding properties emerging from the so-called size effects.[4–9] Some of these outstanding properties accompanying the size reduction are related to the transition to a single domain magnetic structures. While constant efforts are routinely being made for the development of new methods for the synthesis of nanophase magnetic materials in a more efficient and economical way,[3–5,10–25] the attempts have to continue to characterize them structurally using techniques with a probe size of atomic dimension so that unambiguous information can be obtained.[26–28]

The elucidation of atomic structure becomes key for the understanding of physical properties especially when the size of the crystallites is progressively reduced from macroscopic dimension down to the scale of a few nanometers. In the materials constituted of crystals of nanometer dimension, interfaces are created in which the local atomic arrangements (short-range order) are different from those of the crystal lattice. As the grain size is reduced, the number of interfaces increases, and the fraction of atoms on the interface sites becomes comparable to the number of crystal lattice atoms. Hence, the overall properties of the solid are no longer determined by the atomic interactions in the crystal lattice alone. Instead, the material can have properties reflecting the contribution from the interfaces. Besides, the atomic structure in the interior of crystallites is modified through the introduction of defects, strain fields, or short-range correlated static or dynamic displacements of atom from their ideal lattice position. In addition, nanometer-sized isolated crystallites and bulk nanocrystalline solids can differ from macroscopic crystals with respect to their crystallographic phase and their lattice constant. Many properties will reflect the combined effect of these structural changes, that is of the reduction of the length scale on which there is coherency in atomic arrangement (long-range order), of the modified crystallographic structure, and of the introduction of interfaces with an atomic short-range order different from the one in crystal lattice.

It is in this context that we have conducted investigations focused on (i) the fabrication of single domain nickel nanocrystals, (ii) characterization of their atomic structure using scanning transmission electron microscopy with atomic number (Z) contrast (STEM-Z) in conjunction with electron energy loss spectroscopy (EELS), and (iii) magnetic property of these single domain nanomagnets.

Nanocrystalline nickel crystallites were embedded in an alumina matrix using a KrF excimer laser (252 nm, 30 ns full width at half maximum) focused alternately onto high-purity targets of nickel and alumina. The depositions were carried out on silicon substrates in a high vacuum environment ($\sim 5\times10^{-7}$ Torr) at a substrate temperature of approximately 500 °C, an energy density of 2 J/cm^2 and repetition rate of 10 Hz.

Shown in Fig. 1 is a STEM-Z image of the Ni nanocrystals embedded in the alumina matrix. Z-contrast imaging was carried out in a 300 kV VG Microscopes HB603U. In the

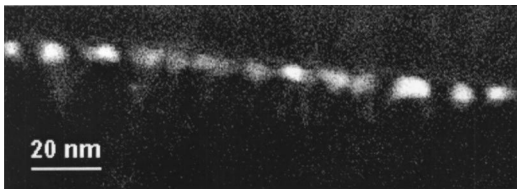

FIG. 1. A STEM-Z image of the Ni nanocrystals embedded in the alumina matrix.

[a]On leave from: North Carolina A & T State University, Greensboro, NC 27411; electronic mail: dkumar@ncat.edu

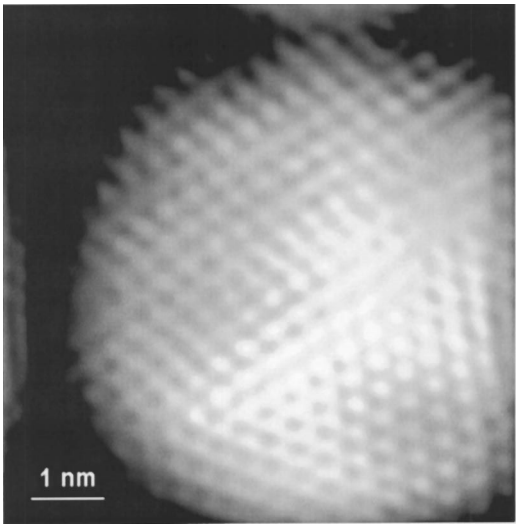

FIG. 2. A high-resolution STEM-Z image of a single Ni nanocrystal and adjoining alumina matrix.

Z-contrast imaging technique, transmitted electrons are detected by a high-angle annular dark-field detector. A high-resolution STEM-Z image of a single Ni nanocrystal and adjoining alumina matrix is shown in Fig. 2. It is clear from this image that the Ni particle is well crystalline and the interface is very abrupt. We also see some defects within the Ni particle. From this image, it appears that the Ni lattice continues to the edge of the nanoparticle, suggesting no oxide has been formed.

EEL spectra collected on a 100 kV HB501UX STEM confirm that no oxide shell was formed. Spectra were obtained while scanning a line across the particle and acquiring the annular dark-field signal simultaneously. In this way, the position of the probe for each EEL spectrum was known to atomic precision. In particular, because the probe size is only 0.2 nm, it is simple to locate the edge of the nanoparticles directly from the line scan. With such a small probe size, Ni EELS data from this probe position are highly sensitive to the nanoparticle surface layer. Allowing for surface curvature, we estimate approximately 50% contributions from the surface monolayer and the bulk Ni in the nanoparticles interior. The energy resolution of the parallel energy loss spectrometer, as determined by the full width half maximum of the zero-loss peak, was 1.1 eV and the dispersion was 0.303 eV/channel over 385 channels. Each spectrum was corrected for the gain variation across the detector array and the background was fitted to a power low over a 50 eV window preceding the edge onset and subtracted from each spectrum. Spectra from the center and edge of a single Ni particle are displayed in Fig. 3. After scaling for intensity differences, the two spectra superimpose precisely, demonstrating the presence of pure metallic Ni at the surface. A comparison of these spectra with the metallic Ni reference spectrum also indicates metallic Ni.[29] We estimate this to be less than 0.1 monolayer of oxide based on the statistics in the spectra. Also shown in Fig. 3 is the background spectrum which was subtracted from both the center and edge spectra. The small uncertainity in the estimation of oxide layer on Ni particles comes from the size of the electron probe used in the present EELS study which is 1.2 Å.

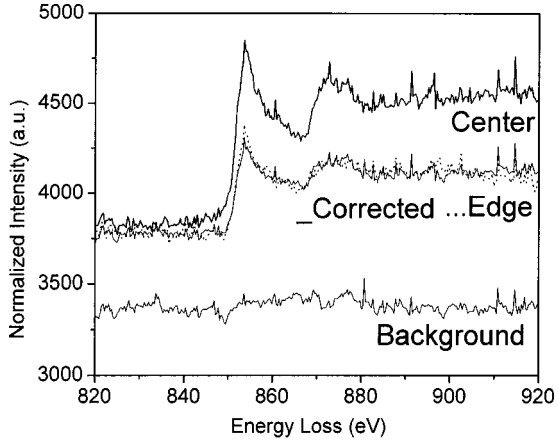

FIG. 3. EEL Spectra from the center and edge of a single Ni particle. Shown also is the background spectrum.

Magnetic measurements were carried out with a superconducting quantum interference device magnetometer (Quantum Design). The zero-field-cooled (ZFC) and field-cooled (FC) magnetization (M) as a function of temperature (T) are shown in Fig. 4 for a $Ni-Al_2O_3$ sample. The ZFC magnetization was achieved by applying a field of 500 Oe to the sample at 10 K and then warming the sample in the constant field with the magnetization being measured as a function of temperature. The FC magnetization was measured by cooling the sample to 10 K in the presence of a 500 Oe field and taking the data while heating the samples up to 350 K. In ZFC mode, the magnetization increases at first, then decreases with an increase in temperature. The temperature at which the maximum in ZFC magnetization occurs, is characterized as the blocking temperature (T_B). As a typical blocking behavior of superparamagnetic particles, the Ni nanocrystals show a different magnetization process when the sample is cooled below the blocking temperature with an external field.[30] The FC magnetization increases monotonically with the decrease in temperature. Ni nanoparticles also show a typical hysteresis behavior for their field-dependent magnetization below the blocking temperature as seen in the top inset of Fig. 4. The value of coercivity obtained from the curve is 150 Oe at 10 K. An estimate of the average magnetic size is obtained from the slope of the magnetization near

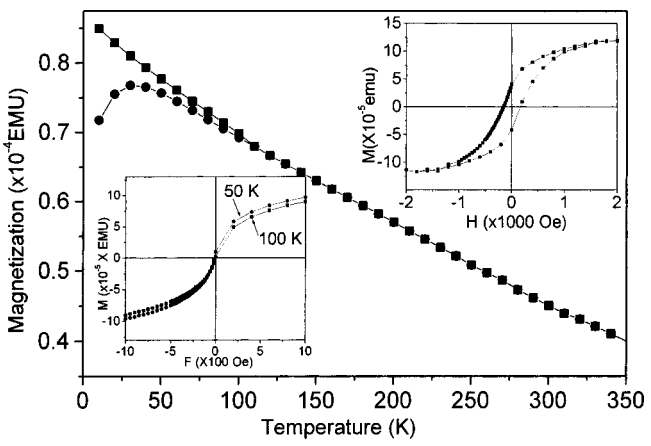

FIG. 4. ZFC and FC magnetization as a function of temperature for a $Ni-Al_2O_3$ sample. $M-H$ loops at 10 K (top inset), 50 and 100 K (bottom inset).

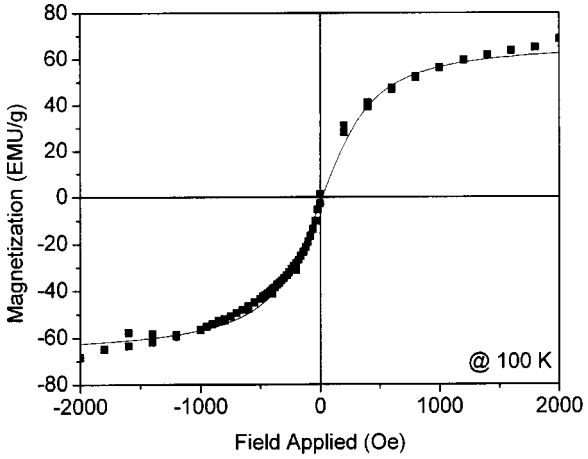

FIG. 5. The best fit for the Langevin function at 100 K.

zero field, the major contribution to which comes from the largest particles. Therefore, an upper bound for the magnetic size may be estimated using the data in the top inset of Fig. 4 and the following equation,[31]

$$D_m = \left[\frac{18 k_{bT}}{\pi} \frac{(dM/dH)_{H=0}}{\rho M_s^2} \right]^{1/3}, \tag{1}$$

where D_m is the maximum diameter, k_b is the Boltzmann constant, T is the temperature (100 K), dM/dH = slope near zero field (0.175 emu/g Oe), and ρ is the density of Ni (8.9 g/cm^3). The initial slope near the origin was determined from the hysteresis plots by curve fitting the linear portion of the data. Inserting the value of saturation magnetization M_s from the above curve fitting (67 emu/g), the magnetic diameter of the particle is found to be 7 nm. This is exactly the average diameter estimated from STEM-Z measurements. Such an excellent correlation between the magnetic size and the physical size of the particles indicates the absence of any magnetically dead layers on the Ni particles.

Above the blocking temperature, the typical characteristics of superparamagnetic behavior are observed showing almost immeasurable coercivity and remanence at 50 and 100 K (bottom inset of Fig. 4). For superparamagnetic particles, the true magnetic moment at a particular temperature can be calculated using the Langevin function[32]

$$M = M_s \left(\coth\left(\frac{\mu H}{k_b T} \right) - \frac{k_b T}{\mu H} \right), \tag{2}$$

where μ is the true magnetic moment of each particle, k_b is the Boltzmann constant, T is the absolute temperature, and M_s is the saturation magnetization. Figure 5 shows the best fit for the Langevin function in the equation at 100 K. From this data fitting, the mean-magnetic moment per Ni nanocrystal is found to be 9074 μ_B, which yields a magnetic moment of 0.64 μ_B per atom. This value of magnetic moment per atom is in excellent agreement with the theoretical value of magnetic moment of Ni atom (0.60 μ_B per atom).

In summary, we have demonstrated the controlled fabrication of superparamagnetic Ni nanocrystals of a few nanometers embedded in an insulating matrix using the pulsed-laser deposition process. The structural characterizations carried out using STEM-Z and EELS have revealed that the Ni particles are well separated from each other and the interfaces between the particle and the host matrix are free of Ni oxide layers within an experimental error of 0.1 monolayer which is an important factor for the realization of good magnetic properties.

This research was sponsored by the Division of Materials Sciences, U.S. Department of Energy, under Contract No. DE-AC05-00OR22725 managed by UT-Battelle, LLC, and by the US National Science Foundation under through the CREST program.

[1] V. F. Puntes, K. M. Krishnan, and P. Alivisatos, Appl. Phys. Lett. **78**, 2187 (2001).
[2] J. L. Dorman, D. Fiorani, and E. Tronc, Adv. Chem. Phys. **98**, 283 (1997).
[3] D. Kumar, H. Zhou, T. K. Nath, A. V. Kvit, and J. Narayan, Appl. Phys. Lett. **79**, 2817 (2001).
[4] D. Kumar, J. Narayan, T. K. Nath, A. K. Sharma, A. Kvit, and C. Jin, Solid State Commun. **119**, 63 (2001).
[5] D. Kumar, J. Narayan, A. V. Kvit, A. K. Sharma, and J. Sankar, J. Magn. Magn. Mater. **232**, 161 (2001).
[6] A. S. Edelstein and R. C. Cammarata, *Nanomaterials: Synthesis, Properties and Applications* (Institute of Physics, Bristol, 1998).
[7] W. Luo, S. R. Nagel, T. F. Rosenbaum, and R. E. Rosensweig, Phys. Rev. Lett. **67**, 2721 (1991).
[8] R. W. Chantrell, N. S. Walmsey, J. Gore, and M. Maylin, Appl. Phys. Lett. **85**, 4320 (1999).
[9] J. Gonzalo, R. Serna, C. N. Afonso, J. Bosbach, T. Wenzel, F. Stietz, F. Tranger, D. Babonneau, and D. E. Hole, J. Appl. Phys. **89**, 5734 (2001).
[10] J. R. Childress, C. L. Chien, and M. Nathan, Appl. Phys. Lett. **56**, 95 (1990).
[11] H. Akinaga, S. Miyanishi, K. Tanaka, W. Van Roy, and K. Onodera, Appl. Phys. Lett. **76**, 97 (2000).
[12] G. Xiao and C. L. Chien, Appl. Phys. Lett. **51**, 1280 (1987).
[13] S. Linderoth and M. S. Pedersen, J. Appl. Phys. **75**, 5867 (1994).
[14] S. P. Li, W. S. Lew, Y. B. Xu, A. Hirohata, A. Samad, F. Baker, and J. A. C. Bland, Appl. Phys. Lett. **76**, 748 (2000).
[15] M. Dahlgren and R. Gorssinger, Mater. Sci. Forum **302**, 263 (1999).
[16] C. L. Chien, in *Science and Technology of Nanostructured Materials*, edited by G. C. Hadjipanayis and G. A. Prinz (Plenum, New York, 1991), p. 477.
[17] M. E. McHenry, S. A. Majetich, J. O. Artman, M. DeGraef, and S. W. Staley, Phys. Rev. B **49**, 11 358 (1994).
[18] S. Wirth and S. von Molnar, J. Appl. Phys. **87**, 7010 (2000).
[19] J. M. Meldrim, Y. Qiang, Y. Liu, H. Haberland, and D. J. Sellmyer, J. Appl. Phys. **87**, 7013 (2000).
[20] B. Bian, D. Laughlin, K. Sato, and Y. Hirotsu, J. Appl. Phys. **87**, 6962 (2000).
[21] E. S. Murdock, R. F. Simmons, and R. Davidson, IEEE Trans. Magn. **28**, 3078 (1992).
[22] S. Roy, B. Roy, and D. Chakravorty, J. Appl. Phys. **79**, 1642 (1996).
[23] I. Navarro, E. Pulido, P. Crespo, and A. Hernando, J. Appl. Phys. **73**, 6525 (1993).
[24] A. Marchand, B. Barbara, P. Mollard, G. Fillion, X. Devaux, and A. Rousset, J. Magn. Magn. Mater. **116**, 64 (1992).
[25] C. W. Teng, J. F. Muth, R. M. Kolbas, K. M. Hassan, A. K. Sharam, A. Kvit, and J. Narayan, Appl. Phys. Lett. **76**, 43 (2000).
[26] A. J. Mcgibbon, S. J. Pennycook, and J. E. Angelo, Science **269**, 519 (1995).
[27] S. J. Pennycook and J. Narayan, Phys. Rev. Lett. **54**, 1543 (1985).
[28] S. J. Pennycook, Annu. Rev. Mater. Sci. **22**, 171 (1992).
[29] E. C. Dickey, X. Fan, and S. J. Pennycook, Acta Mater. **47**, 4061 (1999).
[30] B. D. Cullity, *Introduction to Magnetic Materials* (Addison–Wesley, Massachusetts, 1972).
[31] E. E. Carpenter, J. Magn. Magn. Mater. **225**, 17 (2001).
[32] D. K. Kim, Y. Zhang, W. Voit, K. V. Rao, and M. Muhammed, J. Magn. Magn. Mater. **225**, 30 (2001).